ACS Chemical Neuroscience

Article

Development of a PET Radiotracer for Imaging Elevated Levels of Superoxide in Neuroinflammation

Catherine Hou, Chia-Ju Hsieh, Shihong Li, Hsiaoju Lee, Thomas J. A. Graham, Kuiying Xu, Chi-Chang Weng, Robert K. Doot, Wenhua Chu, Subhasish K. Chakraborty, Laura L. Dugan, Mark A. Mintun, and Robert Mach

ACS Chem. Neurosci., **Just Accepted Manuscript** • DOI: 10.1021/acschemneuro.7b00385 • Publication Date (Web): 03 Nov 2017

ACS Publications

ACS Chemical Neuroscience is published by the American Chemical Society. 1155 Sixteenth Street N.W., Washington, DC 20036

Development of a PET Radiotracer for Imaging Elevated Levels of Superoxide in Neuroinflammation

Catherine Hou,[1] Chia-Ju Hsieh,[1] Shihong Li,[1] Hsiaoju Lee,[1] Thomas J. Graham,[1] Kuiying Xu,[1] Chi-Chang Weng,[1] Robert K. Doot,[1] Wenhua Chu,[2] Subhasish K. Chakraborty,[3] Laura L. Dugan,[3] Mark A. Mintun,[2] Robert H. Mach[1]

[1]Department of Radiology, Perelman School of Medicine, University of Pennsylvania, Philadelphia, PA

[2]Mallinckrodt Institute of Radiology, Washington University School of Medicine, St. Louis, MO

[3]Department of Medicine, Vanderbilt University School of Medicine, Nashville, TN

Keywords: reactive oxygen species, superoxide, positron emission tomography, neuroinflammation

Corresponding author:

Robert H. Mach, Ph.D.
Britton Chance Professor of Radiology
University of Pennsylvania
Chemistry Building, Room 283
231 S. 34th St
Philadelphia, PA 19104
Email: rmach@mail.med.upenn.edu

ABSTRACT

Reactive oxygen species (ROS) are believed to play a major role in the proinflammatory, M1-polarized form of neuroinflammation. However, it has been difficult to assess the role of ROS and their role in neuroinflammation in animal models of disease because of the absence of probes capable of measuring their presence with the functional imaging technique positron emission tomography (PET). This study describes the synthesis and in vivo evaluation of [^{18}F]ROStrace, a radiotracer for imaging superoxide in vivo with PET, in an LPS model of neuroinflammation. [^{18}F]ROStrace was found to rapidly cross the blood-brain barrier (BBB) and was trapped in the brain of LPS-treated animals but not the control group. [^{18}F]*ox*-ROStrace, the oxidized form of [^{18}F]ROStrace, did not cross the BBB. These data suggest that [^{18}F]ROStrace is a suitable radiotracer for imaging superoxide levels in the CNS with PET.

INTRODUCTION

The term reactive oxygen species (ROS) has been used to describe a class of highly reactive oxygen-containing molecules including superoxide radical anion ($O_2^{\bullet -}$), hydrogen peroxide (H_2O_2), hydroxyl radical ($OH^{\bullet -}$) and hypochlorous acid (HOCl).[1-3] While ROS have a role in normal cellular processes, high levels of ROS can lead to oxidative stress and protein, lipid, and DNA damage. Consequently, ROS levels are tightly regulated in a cell through the activity of the enzymes, superoxide dismutase (SOD1, SOD2, SOD3), catalase, and NADH peroxidase.[1, 3] An imbalance between the rate of formation of ROS and the regulatory mechanisms resulting in elevated ROS leads to a condition called oxidative stress.[4] Oxidative stress has been implicated in the pathogenesis of cardiovascular, neurodegenerative diseases and cancer.[1]

One major source of ROS is by oxidative phosphorylation in the mitochondria, and mitochondrial dysfunction involving reduced Complex I activity is considered to be one of the main sources of elevated ROS in Parkinson's Disease (PD).[2, 3] Another main source of ROS are the Nicotinamide Adenine Dinucleotide Phosphate (NADPH) oxidases (NOX1-5, DUOX1-2), which are a family of enzymes that transfer electrons from the reduced form of NADPH to molecular oxygen.[3, 5] The NADPH oxidases have a widespread distribution throughout the body and are thought to play a key role in host defense, cellular signaling, stress response and tissue homeostasis. Within the CNS, NOX1 and NOX4 are expressed in low levels in neurons, astrocytes and microglial cells, whereas NOX2 is expressed in high levels in microglial cells. NOX2 is thought to be latent under normal conditions; upon microglial activation, NOX2 becomes activated through the formation of a multimeric protein complex leading to NOX2-derived superoxide formation.[5] This activation process is thought to play a key role in mediating proinflammatory, M1-polarized microglia in neuroinflammation, and an increase in levels of NOX2 and other markers of oxidative stress have been reported in postmortem samples of

Alzheimer's Disease (AD) brain and in transgenic mouse models of AD.[4, 6] Similar results have been reported in the substantia nigra of PD brain samples and in the 1-methyl-4-phenyl-1,2,3,6-tetrahydropyridine (MPTP) model of PD. In addition, the spinal cord of patients with amyotropic lateral sclerosis (ALS) have been reported to have increased NOX2 expression and other measures of oxidative stress such as the elevation of COX-2 and other cytokines.[7] These results indicate that the proinflammatory form of neuroinflammation leading to the elevation of superoxide and ROS represents a common pathway in neurodegenerative disorders.

Based on the above discussion, an imaging probe capable of measuring levels of superoxide in brain would be a valuable tool for measuring the pro-inflammatory, M1-polarized form of neuroinflammation. Furthermore, since neuroinflammation is thought to represent a hallmark in the pathophysiology of a number of neurodegenerative diseases [7] a PET radiotracer for measuring superoxide levels in the CNS could provide insight into the relationship between the formation of ROS and other pathological features associated with neurodegeneration (e.g., Aβ and tau formation in AD).[8]

The fluorescent probe dihydroethidium (DHE) has been used to measure superoxide levels in cells and tissues using microscopy and optical imaging techniques.[9-11] Our group has previously reported the synthesis of an ^{18}F-labeled analogue of DHE, [^{18}F]FDMT, and its evaluation in an animal model of adriamycin-induced model of cardiotoxicity (Figure 1).[12] The results of this study were significant since it revealed for the first time the ability to image ROS in a living organism using positron emission tomography (PET). While this tracer was able to image ROS levels in peripheral organs in vivo, it did not cross the blood-brain-barrier to allow imaging of elevated superoxide levels associated with proinflammatory microglia activation. In the current study, we report the in vivo evaluation of an ^{18}F-labeled analogue of DHE, [^{18}F]ROStrace (Scheme 1), which is capable of crossing the blood-brain-barrier. We also describe the series

of in vivo validation studies confirming the ability of [^{18}F]ROStrace to image superoxide levels in a murine model of neuroinflammation.

RESULTS

Chemistry and reactivity with reactive oxygen species. The synthesis of ROStrace and its precursor for radiolabeling is shown in Scheme 1. The hydroxyethyl was introduced to the known hydroxy compound di-*tert*-butyl (6-(4-hydroxyphenyl)phenanthridine-3,8-diyl)dicarbamate [12] to form compound **2**, which was methylated with iodomethane, reduced by sodium borohydride and then carefully tosylated to give the precursor compound **3**. The standard compound, ROStrace (**6**), was synthesized (Scheme 1) under a similar procedure. Once the compounds were reduced, they are very labile especially in solution. All the following procedures were performed in a rapid manner under low temperature.

The reactivity of DHE and ROStrace for superoxide, hydrogen peroxide and hydroxyl radical was measured using an in vitro assay as previously reported.[12] Two different methods were used to generate superoxide, xanthine oxidase metabolism of hypoxanthine or by thermal decomposition of 3-morpholinosyndnomine (SIN-1) in the presence of 2-(4-carboxyphenyl)-4,4,5,5,tetramethyl-imidazoline-1-oxyl-3-oxide (CPTIO). In the both systems, oxidation of ROStrace was completely prevented by the addition of superoxide dismutase (SOD) (Figure 2). ROStrace was also exposed to hydrogen peroxide alone or in the presence of horseradish peroxidase (HRP) to generate hydroxyl free radical. The fluorescence intensity results indicate that ROStrace has little reactivity with hydrogen peroxide or hydroxyl radical (Figure 2). These data suggest that ROStrace has good selectivity for superoxide. Since its chemical reactivity is similar to DHE, which is selectively oxidized to ethidium by superoxide radical (Figure 2), we believe ROStrace will behave like DHE in vivo and measure brain levels of superoxide radical.[13]

Radiochemistry. [^{18}F]ROStrace was synthesized (Scheme 2) in an 8-10% radiochemical yield starting from [^{18}F]fluoride ion, with molar activity >74 GBq/μmol. In order to confirm the mechanism of uptake of radioactivity in the LPS-treated mice, [^{18}F]ox-ROStrace was also synthesized. This was accomplished by the quantitative conversion of [^{18}F]ROStrace to [^{18}F]ox-ROStrace by treatment with cupric sulfate (Scheme 2).

In vivo evaluation. The in vivo evaluation of [^{18}F]ROStrace was performed using an LPS-treated mouse model of neuroinflammation. MicroPET imaging studies were conducted in both control (N = 15) and LPS-treated animals (N = 16). The sagittal images revealed a much higher brain uptake of [^{18}F]ROStrace in the LPS-treated animals relative to the control group (Figure 3a). Time-activity curves from the control mice demonstrated that [^{18}F]ROStrace has a high initial brain uptake, peaking within the first minute, followed by a rapid washout. In LPS-treated animals, activity continued to increase in the brain, peaking around three minutes post-injection (Figure 3b). Levels of brain activity in both control and LPS-treated mice stabilized after about 20 minutes. However, the retention of radioactivity in brain was higher in the LPS-treated mice.

The initial analysis of the group data involved a comparison of the average %ID/cm^3 from 40 – 60 min post-injection of the radiotracer for the control versus LPS-treated animals. This time interval was chosen because it represents a plateau phase in the time-activity curves. A graph of the average %ID/cm^3 for the two groups (Figure 3c) revealed a statistically significant difference between the control and LPS-treated animals ($P < 0.0001$) even though there was some overlap between individual subjects in the LPS-treated group and the control group. When the LPS-treated mice were grouped as a whole and compared to the control group, a 156% increase in brain uptake was observed.

It was also observed that not all animals responded to the LPS-treatment in the same manner. That is, some animals displayed more severe symptoms than others, while others appeared to be unaffected by the dose of LPS. In order to characterize the animals to the degree of "sickness" following the LPS-treatment, a scoring mechanism based on criteria outlined by Carstens and Moberg[14] for recognizing pain and distress in laboratory animals was used. Using this method, animals were assigned a condition score based on visual observation of signs of distress including hunched posture, decreased motion, piloerection, lack of grooming, and discharge from the eyes. The animals were then grouped into three levels of sickness: level 1 animals displayed mild symptoms and appeared fairly normal; level 2 animals displayed a moderate response including some of the stated symptoms; level 3 animals displayed practically all the symptoms and with more severity. The results of this analysis are shown in Figure 4. Animals with a condition score of 2 or 3 had a significantly higher uptake of [^{18}F]ROStrace relative to the control group and level 1 animals. These data indicate that the difference in response to LPS as measured via the observational studies is predictive of the relative amount of neuroinflammation in the CNS.

To further confirm the mechanism of retention of [^{18}F]ROStrace in the CNS, radiometabolite analysis of homogenates from brains obtained after completion of the microPET imaging studies was conducted. The results of the HPLC studies indicated that the activity in brain was primarily the oxidized species, [^{18}F]ox-ROStrace, while a much smaller amount of the parent compound was detected (68% vs 10%) 2 hr after an iv injection of [^{18}F]ROStrace. Blood levels of the oxidized species are much lower (27%) at the same time point, suggesting that [^{18}F]ox-ROStrace is not entering the brain from the circulation (Table 1).

We believe the neutral species, [^{18}F]ROStrace, enters the brain where it is trapped upon oxidation to [^{18}F]*ox*-ROStrace by superoxide. To demonstrate that the higher retention of

[^{18}F]ROStrace in LPS-treated mice is due to oxidation by LPS-induced ROS in the brain, and that the peripherally oxidized species, [^{18}F]*ox*-ROStrace, is not able to enter the brain, mice were imaged after an injection of [^{18}F]*ox*-ROStrace. [^{18}F]*ox*-ROStrace showed no brain uptake in the untreated mice (Figure 5). These data demonstrate that the neutral species, [^{18}F]ROStrace, crosses the blood-brain barrier and is oxidized to [^{18}F]ox-ROStrace after entering the brain. LPS treatment is known to cause some disruption of the blood brain barrier, and our LPS-treated mice displayed a small amount of brain uptake when injected with [^{18}F]ox-ROStrace at 24 hours post LPS treatment. The same imaging procedure performed one week after LPS treatment resulted in no uptake. These data confirm the trapping mechanism of [^{18}F]ROStrace in the brain is due to oxidation by superoxide to [^{18}F]*ox*-ROStrace (Figure 5).

Ex vivo autoradiography studies were conducted on brain sections harvested after completion of the PET imaging studies. In these studies, animals were injected with DHE (15 mg/kg, i.v.) 30 min prior to sacrifice so that a comparison can be made between the distribution of the radiotracer, which is primarily [^{18}F]*ox*-ROStrace and the fluorescent signal from oxidized DHE (i.e., ethidium / 2-OH-ethidium). The results of this study indicate a similar pattern of distribution between the radiotracer and oxidized DHE fluorescence (Figure 6). We also obtained fluorescence images in mice 30 minutes after injection of cold ROStrace (14 mg/kg, i.v.). As expected, this also provided a similar pattern of distribution in the brain. These results further support the mechanism of uptake and trapping of [^{18}F]ROStrace in the CNS under conditions of elevated ROS.

DISCUSSION

The goal of this study was to develop a PET radiotracer for imaging superoxide levels in the CNS that are produced during the proinflammatory, M1-polarized form of neuroinflammation that is thought to be a hallmark feature of neurodegeneration.[7, 8, 15] Our group previously

reported an ^{18}F-labeled analogue of the fluorescent probe DHE and demonstrated that it was capable of imaging superoxide that is produced in myocardial tissues in an animal model of Adriamycin-induced cardiotoxicity.[12] Although this probe is capable of imaging superoxide in peripheral organs, its inability to cross the blood-brain barrier prevented its use as a means of imaging superoxide produced under conditions of neuroinflammation and mitochondrial dysfunction which are thought to occur in most neurodegenerative disorders.

In the time interval between our initial publication and this current study, a number of ROS-based radiotracers have been reported in the literature. These include: 1) [^{18}F]PC-FLT, which measures extracellular and intracellular levels of H_2O_2;[16] 2) [^{11}C]Vitamin-C, which measures extracellular levels of H_2O_2;[17] 3) the hydrocyanine dye derivative, [^{18}F]ROS1, which measures superoxide and hydroxyl radicals;[18] 4) [^{18}F]5-Fluoroaminosuberic acid, which provides an indirect measure of intracellular levels of ROS by imaging the increase in expression of the cystine transporter (system x_c-);[19] and 5) [^{11}C]DHQ1, a dihydroisoquinoline analogue capable of measuring intracellular levels of superoxide.[20] [^{11}C]DHQ1 is capable of crossing the blood-brain barrier and has potential for imaging increased ROS levels in the CNS as a consequence of neuroinflammation.[20] A number of radiolabeled analogues of dihydro-methidium (a.k.a, hydromethidine) have been synthesized and evaluated in vitro and in vivo, including [^{3}H]hydromethidine and [^{11}C]hydromethidine.[21, 22] [^{3}H]Hydromethidine is oxidized by superoxide and hydroxyl radicals and has been evaluated in animal models of stroke and cisplatin-induced nephrotoxicity.[23, 24] A recent paper on the radiosynthesis and preliminary in vivo evaluation of [^{11}C]methidium has also been reported.[22] It should also be noted that our group reported the in vitro properties of methidium towards various forms of ROS in the patent literature (US 9,035,057), but did not pursue radiolabeling this compound because of our interest in developing an ^{18}F-labeled radiotracer for imaging ROS.

In the current study, we report the synthesis, in vitro characterization, and in vivo evaluation of [^{18}F]ROStrace in an LPS-treatment model of neuroinflammation. In vitro studies indicate that it is oxidized to the charged species, [^{18}F]*ox*-ROStrace, by superoxide since it has low reactivity for hydrogen peroxide and hydroxyl radical (Figure 2). Our in vivo studies included not only the uptake of the parent radiotracer, [^{18}F]ROStrace, in LPS-treated versus control mice, but a detailed metabolite analysis study confirming the mechanism of uptake and trapping of the radiotracer in the CNS. This trapping mechanism was also confirmed by the observation that the oxidized species, [^{18}F]*ox*-ROStrace, is not capable of crossing the blood-brain barrier. The distribution of radioactivity in the LPS-treated animals also matched the distribution of the fluorescence signal from treatment of the animals post-PET with DHE, which further supports the mechanism of trapping of the radiotracer in the CNS. Our results revealed that the relative uptake and retention of [^{18}F]ROStrace correlated with the level of sickness induced by LPS, which suggest that this radiotracer is capable of measuring different levels of neuroinflammation in rodent models of neurodegeneration. Taken collectively, our data demonstrates that [^{18}F]ROStrace is the first ^{18}F-labeled radiotracer capable of measuring elevated levels of superoxide which occur during the “neurotoxic” or proinflammatory form of neuroinflammation.

CONCLUSION

[^{18}F]ROStrace is a promising PET radiotracer for imaging elevated superoxide levels in the CNS under conditions of neuroinflammation. We are currently using this radiotracer in a panel of transgenic mouse models of AD, PD and other neurodegenerative disorders.

METHODS

General. All chemicals were purchased from commercial sources and were used without further purification. NMR spectra were taken on a Bruker DMX 500 MHz. Mass spectroscopy data and compound purity analysis were acquired using ESI technique on 2695 Alliance LCMS.

Purification of target compounds were carried out on a Biotage Isolera One with a dual-wavelength UV-VIS detector. Chemical shifts (δ) in the ^{1}H-NMR spectra were referenced by assigning the residual solvent peaks. Elemental analyses were performed by Atlantic Microlabs, Inc. (Atlanta, GA) and were within ± 0.4% unless otherwise noted. Measurement of reactivity for ROS was conducted using the published method.[12]

Di-tert-butyl (6-(4-(2-hydroxyethoxy)phenyl)phenanthridine-3,8-diyl)dicarbamate (1). Di-*tert*-butyl (6-(4-hydroxyphenyl)phenanthridine-3,8-diyl)dicarbamate [12] (501 mg, 1 mmol), 2-bromoethanol (400 mg, 3.22 mmol), potassium carbonate (690 mg, 5 mmol) and DMF (6 mL) were put in a sealed vial and heated to 95°C overnight. The mixture was diluted with water (50 mL) and extracted with ethyl acetate. The organic layer was washed with H_2O/NaHCO3 aqueous/brine (2 x each) and dried with Na_2SO_4. After filtration, the filtrate was condensed and the residue was applied to FC (dichloromethane/ethyl acetate 0-40%) yielding compound **1** (340 mg, 62%) and the recovered starting material. ^{1}H NMR (500 MHz, DMSO-d_6) δ ppm 1.45 (s, 9 H), 1.51 (s, 3H), 3.79 (dt, *J* = 5.1, 4.9 Hz, 2H), 4.11 (t, *J* = 4.9 Hz, 2H), 4.92 (t, *J* = 5.5 Hz, 1H), 7.13 (d, *J* = 8.6 Hz, 2H), 7.65 (d, *J* = 8.6 Hz, 2H), 7.77 (dd, *J* = 8.9, 2.0 Hz, 1H), 8.00 (d, *J* = 8.6 Hz, 1H), 8.17 (s, 1H), 8.25 (s, 1H), 8.56 (d, *J* = 9.1 Hz, 1H), 8.67 (d, *J* = 9.2 Hz, 1H), 9.67 (s, 1H), 9.69 (s, 1H). ^{13}C NMR (500 MHz, DMSO-d_6) δ ppm 28.06, 28.12, 59.59, 69.69, 79.34, 114.11, 115.13, 116.29, 118.14, 118.69, 122.46, 122.67, 122.93, 124.38, 128.10, 131.04, 131.86, 138.08, 139.45, 143.31, 152.76, 152.78, 159.06, 159.83. HRMS: Calcd. for $C_{31}H_{36}N_3O_6^+$ $[M+H]^+$ 546.2599. Found 546.2626.

*2-(4-(3,8-Bis((tert-butoxycarbonyl)amino)-5-methyl-5,6-dihydrophenanthridin-6-yl)phenoxy)ethyl 4-methylbenzenesulfonate (**3**).* Compound **2** (120 mg, 0.22 mmol) was suspended in a mixture of toluene (9 mL) and iodomethane (1 mL) and kept stirring at 70°C overnight. The mixture was condensed under vacuum and the residue was dissolved in 5 mL of methanol. The mixture was

cooled with ice bath and excess of $NaBH_4$ (~30 mg) was added. The mixture was kept stirring at 0°C for 10 min and condensed under vacuum below 10°C. The residue was applied to a pre-equilibrated column of silica and eluted with dichloromethane/ethyl acetate (0-40%). The combined fractions were condensed below 10°C yielding the methylated compound (67 mg, 54%) as slightly brown solid. This compound (67 mg, 0.12 mmol) was then dissolved in dichloromethane (3 mL) under 0°C, p-toluenesulfonyl chloride (84 mg, 0.44 mmol) and trimethylamine (120 mg, 1.2 mmol) were added. The reaction was stirred at 0°C for 2 hr and the reaction mixture was applied to a pre-equilibrated column of silica gel and eluted with dichloromethane /ethyl acetate (0-15%). The proper fractions were combined and condensed below 10°C yielding the title compound as a slightly red solid (65 mg, 76%). ^{1}H NMR (500 MHz, $CDCl_3$) δ ppm 1.48 (s, 9 H), 1.50 (s, 3H), 2.40 (s, 3H), 2.83 (s, 3H), 4.01 (t, *J* = 4.8 Hz, 2H), 4.28 (t, *J* = 4.8 Hz, 2H), 4.92 (t, *J* = 5.5 Hz, 1H), 5.22 (s, 1 H), 6.47 (s, 2H), 6.54 (d, *J* = 8.7 Hz, 2H), 6.72 (s, 2H), 6.98 (d, *J* = 8.7 Hz, 2H), 7.15 (s, 1H), 7.17 (s, 1H), 7.28 (d, *J* = 8.1 Hz, 2H), 7.57 (d, *J* = 8.8 Hz, 1H), 7.64 (d, *J* = 9.0 Hz, 1H), 7.76 (d, *J* = 8.3 Hz, 2H). ^{13}C NMR (500 MHz, $CDCl_3$) δ ppm 21.56, 28.29, 28.33, 37.06, 65.29, 67.18, 68.04, 80.30, 80.45, 102.35, 107.54, 114.45, 116.34, 117.01, 117.86, 122.66, 123.03, 125.50, 127.92, 127.97, 128.10, 128.95, 129.77, 132.84, 134.35, 135.72, 137.01, 139.14, 144.86, 152.52, 157.38. HRMS: Calcd. for $C_{39}H_{46}N_3O_8S^+$ $[M+H]^+$ 716.3000. Found 716.3016.

Di-tert-butyl (6-(4-(2-fluoroethoxy)phenyl)phenanthridine-3,8-diyl)dicarbamate (4). Di-tert-butyl (6-(4-hydroxyphenyl)phenanthridine-3,8-diyl)dicarbamate[1] (1.04 g, 2.07 mol) was dissolved in MeCN, 2-fluoroethyltosylate (902 mg, 4.14 mmol) and K_2CO_3 (855 mg, 6.22 mmol) were added. The reaction was heated to 80°C and allowed to stir overnight. The reaction mixture was filtered and concentrated to give a residue that was purified by FC (DCM/Ethyl acetate 0-50%) to afford the desired compound as off-white foam (800mg, 70%). ^{1}H NMR (500 MHz, DMSO-d_6) δ ppm 1.45 (s, 9H), 1.51 (s, 9H), 4.36 (dt, *J* = 30.1, 3.8 Hz, 2H), 4.81 (dt, *J* = 47.9, 3.8Hz, 2H), 7.16 (d,

J = 8.7 Hz, 2H), 7.66 (d, *J* = 8.7 Hz, 2H), 7.77 (dd, *J* = 9.0, 2.2 Hz, 1H), 8.00 (d, *J* = 8.7 Hz, 1H), 8.56 (d, *J* = 9.1 Hz, 1H), 8.67 (d, *J* = 9.1 Hz, 1H), 9.67 (s, 1H), 9.69 (s, 1H). ^{13}C NMR (500 MHz, DMSO-d_6) δ ppm 28.08, 28.14, 67.15, 67.31, 79.38, 81.52, 82.85, 114.18, 115.06, 116.27, 118.18, 118.73, 122.54, 122.69, 123.01, 124.39, 128.12, 131.14, 132.32, 138.13, 139.49, 143.32, 152.78, 152.81, 158.52, 159.79. HRMS: Calcd. for $C_{31}H_{35}FN_3O_5$ $[M+H]^+$ 548.2555; Found 548.2545.

Di-tert-butyl (6-(4-(2-fluoroethoxy)phenyl)-5-methyl-5,6-dihydrophenanthridine-3,8-diyl)dicarbamate (5). A screw-cap vial containing a solution of Di-tert-butyl (6-(4-(2-fluoroethoxy)phenyl)phen-anthridine-3,8-diyl)dicarbamate (4, 45 mg, 0.082 mmol) in toluene (1.5 mL) was treated with 0.50 mL of iodomethane. The vial was briefly purged with nitrogen, sealed and heated to 95°C for 6 h. The reaction mixture was then moved to a 75°C bath and allowed to stir overnight. The reaction mixture was condensed and taken up in EtOH (2 mL). The solution was treated with excess $NaBH_4$ (7 mg) and concentrated to give a residue that was purified by FC (DCM/Ethyl acetate 0-30%) to give the desired product as a colorless solid (35 mg, 75%). ^{1}H NMR (500 MHz, $CDCl_3$) δ ppm 1.48 (s, 9H), 1.50 s, 9H), 2.85 (s, 3H), 4.08 (dt, *J* = 30.1, 4.2 Hz, 2H), 4.67 (dt, *J* = 47.4, 4.2 Hz, 2H), 5.24 (s, 1H), 6.45 9s, 1H), 6.46 (s, 1H), 6.69-6.73 (m, 4H), 7.03 (d, *J* = 8.7 Hz, 2H), 7.58 (d, *J* = 8.1 Hz, 1H), 7.66 (d, *J* = 8.7 Hz, 1H). ^{13}C NMR (500 MHz, $CDCl_3$) δ ppm 28.30, 28.34, 37.08, 66.86, 67.03, 67.20, 80.42, 80.73, 81.16, 82.52, 102.36, 107.48, 114.48, 117.04, 117.84, 122.69, 123.05, 125.52, 128.06, 134.15, 135.78, 136.99, 139.11, 144.87, 152.56, 157.80. HRMS: Calcd. for $C_{32}H_{39}FN_3O_5$ $[M+H]^+$ 564.2868; Found 564.2880.

6-(4-(2-Fluoroethoxy)phenyl)-5-methyl-5,6-dihydrophenanthridine-3,8-diamine (6). Di-tert-butyl (6-(4-(2-fluoroethoxy)phenyl)-5-methyl-5,6-dihydrophenanthridine-3,8-diyl)dicarbamate (5, 20 mg, 0.035 mmol) was dissolved in EtOAc (1.5 mL) and concentrated HCl (37%, 0.5 mL) was

added. The reaction mixture was purged with nitrogen and left stirred at r.t. for 30 min. The reaction mixture was neutralized with 7N NH_3 in methanol and concentrated under high vacuum to give a rose-colored solid. The solid was dissolved in DCM and applied to FC (ethyl acetate) to afford the title compound as colorless solid (12 mg, 93%). ^{1}H NMR (500 MHz, $CDCl_3$) δ ppm 2.80 (s, 3H), 4.10 (dt, *J* = 30.2, 4.2 Hz, 2H), 4.68 (dt, *J* = 47.4, 4.2 Hz, 2H), 5.13 (s, 1H), 5.92 (d, *J* = 2.2 Hz, 1H), 6.18 (dd, *J* = 8.1, 2.1 Hz, 1H), 6.34 (d, *J* = 2.4 Hz, 1H), 6.61 (dd, *J* = 8.4, 2.4 Hz, 1H), 6.72 (d, *J* = 8.7 Hz, 2H), 7.05 (d, *J* = 8.7 Hz, 2H), 7.45 (d, *J* = 8.2 Hz, 1H), 7.52 (d, *J* = 8.4 Hz, 1H). ^{13}C NMR (500 MHz, $CDCl_3$) δ ppm 37.03, 66.87, 67.03, 67.43, 81.18, 82.54, 99.52, 104.81, 112.98, 114.27, 114.41, 115.09, 122.17, 122.69, 122.95, 128.09, 134.61, 135.60, 144.47, 144.85, 146.47, 157.70. HRMS: Calcd. for $C_{22}H_{23}N_3OF$ $[M+H]^+$ 364.1820; Found 364.1831.

Radiochemistry. The radiosynthesis of [^{18}F]ROStrace was accomplished on an All-in-One module (Trasis, Belgium) with full automation. Briefly, [^{18}F] fluoride (800 mCi) was produced by proton irradiation of enriched ^{18}O water via the reaction of ^{18}O (p, n) ^{18F} by the Cyclone cyclotron (IBA, Belgium). The [^{18}F] fluoride in ^{18}O water solution is delivered to the hotcell and trapped on a pre-activated Sep-Pak® Light QMA Carb cartridge (Waters) and eluted to the reaction vial by 1 mL eluent containing 2 mg potassium carbonate and 7 mg Kryptofix in a mixture of 0.85 mL acetonitrile and 0.15 mL water. The residual water was evaporated azotropically with 1 mL acetonitrile at 100°C under a stream of nitrogen gas and vacuum. A solution of 4 mg tosylate precursor in 0.6 mL methyl sulfide (DMSO) was added to the reaction vial for a 10 min reaction, followed by a 10 min de-protection with 1.0 mL 1 N HCl. The reaction mixture was cooled to 50 °C and neutralized with 0.8 mL 1 N NaOH. The crude product was diluted with 5 mL mobile phase and passed through an Alumina N Light cartridge (Waters) and a 0.45 μm nylon filter to the HPLC loop for high performance chromatography (HPLC). A Phenomenex Luna C18 (2) semi-preparative column (10 X 250 mm) with mobile

phase acetonitrile/water/TFA (15:85:0.1 in volume) was used for HPLC purification. At a flow rate of 5 mL/min, the product was eluted at 18 min and diluted with water to 21 mL. The intermediate (oxidized byproduct) was then eluted with 65% acetonitrile with water. The diluted product solution was passed through a Sep-Pak® Plus C18 cartridge (Waters). The trapped product was rinsed with water to waste and then eluted with ethanol (0.6 mL, with 0.1% ascorbic acid) followed by 8 mL normal saline to the final production vial through a 0.2 μM nylon filter. After shaking well, the final product is ready for quality control (QC) and animal studies. The yield ranged from 8% to 20% (decay corrected to the start of synthesis) in an average time of 65 min from receipt of ^{18}F-fluoride in ^{18}O water solution from the cyclotron.

For the oxidized analog, [^{18}F]ox-ROStrace, [^{18}F]ROStrace was oxidized by adding 2 mL 25 mM cupric sulfate aqueous solution. HPLC purification utilized a Sunfire C18 column (Waters, 10 x 250mm) with a mobile phase of 35% acetonitrile in 20 mM ascorbic acid solution. The retention time is approximately 10 min with a 5 mL/min flow rate. The enrichment and final formulation is the same as for [^{18}F]ROStrace.

Animal models. All animal studies were performed under protocols approved by the University of Pennsylvania Institutional Animal Care and Use Committee. Balb/c mice (Charles River) were injected ip with 5 mg/kg LPS from E coli 0111:B4 (Sigma Aldrich) 24 hours prior to imaging studies. Mice were maintained on anesthesia of 2% isoflurane and placed on a warm pad for scanning. Animals were euthanized at the completion of the scanning procedure by cervical dislocation and brain and blood extracted for HPLC analysis of the identity of the radioactive species present or autoradiography.

Condition Assessment. The effect of LPS treatment on the animals was evaluated by visual observation of indicators including hunched posture, decreased motion, piloerection, lack of

grooming, and discharge from the eyes. This method was developed by combining different animal condition scoring systems and adapting them for common symptoms of LPS treatment. Condition scores ranged from 0 (normal) to 4 (moribund) and were obtained by scoring each animal for the presence of each indicator and whether it was mild or severe (0, 1 or 2). After all indicators were added together, the possible totals (0 to 10) were subdivided into the final condition scores, 0 - 4. No treated animals were scored 0 or 4 in this study. Animals consistently lost approximately 10% body weight at 24 hrs post-LPS treatment, even level 1 animals, so weight was measured but not included as a factor.

PET imaging. Mouse imaging was performed on the Philips MOSAIC HP small animal PET scanner, developed in collaboration with Philips Medical Systems. Dynamic images were acquired up to 60 minutes, after an i.v. injection of 200-300 μCi [^{18}F]ROStrace or [^{18}F]*ox*-ROStrace**.** Slice thickness was 1/2 mm and FOV 12.8 cm. Data reconstruction was performed using 3D-RAMLA protocol with decay correction turned on and normalization set for efficiency. Time-activity curves were constructed by plotting the normalized percent injected dose per cm^3 (normalized %ID/cm^3) versus time for a region-of-interest encompassing the entire brain. When making comparisons between control and LPS-treated animals, the average %ID/cm^3 tissue for the 40 – 60 min period post-injection of [^{18}F]ROStrace was used since this represents a plateau phase in the time-activity curves (i.e., Δ %ID/cm^3 = 0). Three different regions-of-interests (whole brain, cerebrum and cerebellum) were used for the data analysis shown in Figures 3 and 4.

Ex vivo autoradiography. Immediately after imaging, mice were injected i.v. with 15 mg/kg DHE (Sigma Aldrich) and brains harvested 30 minutes later and sectioned on a cryostat microtome. Sections were exposed to phosphor plates to obtain autoradiographic [^{18}F]ROStrace and fluorescent DHE images (GE Typhoon).

Metabolite analysis. Blood samples and brains were collected from mice immediately post-scan and acetonitrile/PBS (1:1) was added at twice the volume of each sample. The blood solution was vortexed and brains were homogenized with a pellet pestle, followed by centrifugation at 3000 g for 10 min. After separating the supernatant from the pellet, each portion was counted with a gamma counter (Perkin Elmer Wizard 2480) to determine the extraction efficiency. Part of the supernatant (> 200 µL) was diluted with the same volume of water and then filtered with a 0.45 μm nylon filter, and 200 µL of the filtered supernatant was injected into an analytical metabolite HPLC (1200 series, Agilent Technologies) equipped with an Agilent SB-C18 column (5 µm, 25 cm x 4.6 mm) and a fraction collector (Waters). The gradient mobile phase consisted of acetonitrile/0.1% TFA solution and the flow rate was 1 mL/min. A fraction was collected every 30 seconds and counted with the gamma counter or directly with the LabLogic Laura Posi-RAM radiodetector.

Statistical Analysis Methods. Nonparametric Mann-Whitney test was used to compare the normalized %ID/cm^3 difference between control and LPS-treated groups. Multiple group comparison among control and each condition level group was calculated by Nonparametric Kruskal-Wallis test with Dunn's post hoc test. Spearman's rank correlation was used to calculate the correlation between normalized %ID/mm^3 and condition scale in each region-of-interest. P value < 0.05 was considered as a statistically significant difference.

Author Contributions

R.H.M., L.L.D. and M.A.M. conceived of the project; C.H. and R.H.M. managed the study. T.J.G., K.X. and W.C. conducted organic synthesis; S.L. and T.J.G. conducted radiochemistry; S.L. and H.L. performed analytical QC. S.K.C. and L.L.D. conducted the in vitro ROS assay. C.H. prepared the animals and performed the imaging studies; C-C.W. performed the

autoradiography. C-J.H. and R.K.D. processed images and performed the PET data analysis. C.H., C-J.H., S.L., K.X. and R.H.M. wrote the manuscript.

Funding Sources

This research was funded by a grant from the Michael J. Fox Foundation (RHM), and NIH grant AG033679-05 (LLD).

Conflict of Interest

The radiotracer described in this manuscript is covered under US Patent Number 9,035,057 B2 (RHM, WC, LLD, MAM, RHM, inventors). There are no other conflicts of interest.

ACKNOWLEDGEMENT

We thank Eric Blankemeyer and the University of Pennsylvania Small Animal Imaging Facility for assistance with microPET imaging.

REFERENCES

[1] Krumova, K., and Cosa, G. (2016) Chapter 1 Overview of Reactive Oxygen Species, In *Singlet Oxygen: Applications in Biosciences and Nanosciences, Volume 1*, pp 1-21, The Royal Society of Chemistry.

[2] Patten, D. A., Germain, M., Kelly, M. A., and Slack, R. S. (2010) Reactive oxygen species: stuck in the middle of neurodegeneration, *Journal of Alzheimer's disease : JAD 20 Suppl 2*, S357-367.

[3] Sies, H., Berndt, C., and Jones, D. P. (2017) Oxidative Stress, *Annual review of biochemistry 86*, 715-748.

[4] Klein, J. A., and Ackerman, S. L. (2003) Oxidative stress, cell cycle, and neurodegeneration, *The Journal of clinical investigation 111*, 785-793.

[5] Haslund-Vinding, J., McBean, G., Jaquet, V., and Vilhardt, F. (2017) NADPH oxidases in oxidant production by microglia: activating receptors, pharmacology and association with disease, *British journal of pharmacology 174*, 1733-1749.

[6] Ganguly, G., Chakrabarti, S., Chatterjee, U., and Saso, L. (2017) Proteinopathy, oxidative stress and mitochondrial dysfunction: cross talk in Alzheimer's disease and Parkinson's disease, *Drug design, development and therapy 11*, 797-810.

[7] Glass, C. K., Saijo, K., Winner, B., Marchetto, M. C., and Gage, F. H. (2010) Mechanisms underlying inflammation in neurodegeneration, *Cell 140*, 918-934.

[8] Mach, R. H. (2014) New targets for the development of PET tracers for imaging neurodegeneration in Alzheimer disease, *Journal of nuclear medicine : official publication, Society of Nuclear Medicine 55*, 1221-1224.

[9] Gomes, A., Fernandes, E., and Lima, J. L. F. C. (2005) Fluorescence probes used for detection of reactive oxygen species, *Journal of Biochemical and Biophysical Methods 65*, 45-80.

[10] Dugan, L. L., and Quick, K. L. (2005) Reactive oxygen species and aging: evolving questions, *Science of aging knowledge environment : SAGE KE 2005*, pe20.

[11] Dugan, L. L., Ali, S. S., Shekhtman, G., Roberts, A. J., Lucero, J., Quick, K. L., and Behrens, M. M. (2009) IL-6 mediated degeneration of forebrain GABAergic interneurons and cognitive impairment in aged mice through activation of neuronal NADPH oxidase, *PloS one 4*, e5518.

[12] Chu, W., Chepetan, A., Zhou, D., Shoghi, K. I., Xu, J., Dugan, L. L., Gropler, R. J., Mintun, M. A., and Mach, R. H. (2014) Development of a PET radiotracer for non-invasive imaging of the reactive oxygen species, superoxide, in vivo, *Organic & biomolecular chemistry 12*, 4421-4431.

[13] Hall, D. J., Han, S. H., Chepetan, A., Inui, E. G., Rogers, M., and Dugan, L. L. (2012) Dynamic optical imaging of metabolic and NADPH oxidase-derived superoxide in live mouse brain using fluorescence lifetime unmixing, *Journal of cerebral blood flow and metabolism : official journal of the International Society of Cerebral Blood Flow and Metabolism 32*, 23-32.

[14] Carstens, E., and Moberg, G. P. (2000) Recognizing Pain and Distress in Laboratory Animals, *ILAR Journal 41*, 62-71.

[15] Graeber, M. B. (2010) Changing face of microglia, *Science (New York, N.Y.) 330*, 783-788.

[16] Carroll, V., Michel, B. W., Blecha, J., VanBrocklin, H., Keshari, K., Wilson, D., and Chang, C. J. (2014) A boronate-caged [(1)(8)F]FLT probe for hydrogen peroxide detection using positron emission tomography, *Journal of the American Chemical Society 136*, 14742-14745.

[17] Carroll, V. N., Truillet, C., Shen, B., Flavell, R. R., Shao, X., Evans, M. J., VanBrocklin, H. F., Scott, P. J., Chin, F. T., and Wilson, D. M. (2016) [(11)C]Ascorbic and [(11)C]dehydroascorbic acid, an endogenous redox pair for sensing reactive oxygen species using positron emission tomography, *Chemical communications (Cambridge, England) 52*, 4888-4890.

[18] Al-Karmi, S., Albu, S. A., Vito, A., Janzen, N., Czorny, S., Banevicius, L., Nanao, M., Zubieta, J., Capretta, A., and Valliant, J. F. (2017) Preparation of an 18 F-Labeled Hydrocyanine Dye as a Multimodal Probe for Reactive Oxygen Species, *Chemistry (Weinheim an der Bergstrasse, Germany) 23*, 254-258.

[19] Yang, H., Jenni, S., Colovic, M., Merkens, H., Poleschuk, C., Rodrigo, I., Miao, Q., Johnson, B. F., Rishel, M. J., Sossi, V., Webster, J. M., Benard, F., and Schaffer, P. (2017) 18F-5-Fluoroaminosuberic Acid as a Potential Tracer to Gauge Oxidative Stress in Breast Cancer Models, *Journal of nuclear medicine : official publication, Society of Nuclear Medicine 58*, 367-373.

[20] Okamura, T., Okada, M., Kikuchi, T., Wakizaka, H., and Zhang, M. R. (2015) A (1)(1)C-labeled 1,4-dihydroquinoline derivative as a potential PET tracer for imaging of redox status in mouse brain, *Journal of cerebral blood flow and metabolism : official journal of the International Society of Cerebral Blood Flow and Metabolism 35*, 1930-1936.

[21] Abe, K., Takai, N., Fukumoto, K., Imamoto, N., Tonomura, M., Ito, M., Kanegawa, N., Sakai, K., Morimoto, K., Todoroki, K., and Inoue, O. (2014) In vivo imaging of reactive oxygen species in mouse brain by using [3H]hydromethidine as a potential radical trapping radiotracer, *Journal of cerebral blood flow and metabolism : official journal of the International Society of Cerebral Blood Flow and Metabolism 34*, 1907-1913.

[22] Wilson, A. A., Sadovski, O., Nobrega, J. N., Raymond, R. J., Bambico, F. R., Nashed, M. G., Garcia, A., Bloomfield, P. M., Houle, S., Mizrahi, R., and Tong, J. (2017) Evaluation of a novel radiotracer for positron emission tomography imaging of reactive oxygen species in the central nervous system, *Nuclear Medicine and Biology 53*, 14-20.

[23] Takai, N., Abe, K., Tonomura, M., Imamoto, N., Fukumoto, K., Ito, M., Momosaki, S., Fujisawa, K., Morimoto, K., Takasu, N., and Inoue, O. (2015) Imaging of reactive oxygen species using [(3)H]hydromethidine in mice with cisplatin-induced nephrotoxicity, *EJNMMI research 5*, 116.

[24] Abe, K., Tonomura, M., Ito, M., Takai, N., Imamoto, N., Rokugawa, T., Momosaki, S., Fukumoto, K., Morimoto, K., and Inoue, O. (2015) Imaging of reactive oxygen species in focal ischemic mouse brain using a radical trapping tracer [(3)H]hydromethidine, *EJNMMI research 5*, 115.

Table 1

	Polar	[^{18}F]ROStrace	[^{18}F]ox-ROStrace
Brain	7.0 ± 1.9	10.0 ± 2.5	68.3 ± 2.2
Blood	23.8 ± 8.2	31.8 ± 7.3	27.0 ± 2.3

Figure Legends

Figure 1. Structures of Dihydroethidium, [^{18}F]FDMT, and [^{18}F]ROStrace.

Figure 2. DHE and ROStrace are selectively oxidized by superoxide and hydroxyl radicals, but not by H_2O_2. ROStrace was exposed to superoxide (generated by two methods: xanthine oxidase metabolism of hypoxanthine or by thermal decomposition of SIN-1 in the presence of CPTIO); hydrogen peroxide alone; or in the presence of horseradish peroxidase (HRP) to generate hydroxyl free radical. Oxidation of ROStrace was prevented by the addition of superoxide dismutase (SOD).

Figure 3. [^{18}F]ROStrace microPET imaging in control and LPS-treated mice. (A) Representative control and LPS-treated mouse images 40-60 min post [^{18}F]ROStrace injection. (B) Time activity curves demonstrate high initial brain uptake followed by plateau after 40 min. %ID/cm^3 were obtained from 40-60 min summed images (C) to show differential uptake in control vs. LPS-treated mice.

Figure 4. Stratification of LPS-treated mice based on condition score suggests that higher brain uptake of [^{18}F]ROStrace correlates with greater severity of symptoms from LPS treatment.

Figure 5. Demonstration that [^{18}F]ox-ROStrace does not cross the blood brain barrier. (A) Mechanism of brain uptake and retention of [^{18}F]ROStrace. (B) microPET images and time activity curve comparing brain uptake of [^{18}F]ROStrace vs [^{18}F]ox-ROStrace.

Figure 6. The distribution pattern of [^{18}F]ROStrace is comparable with the fluorescent signal from DHE or ROStrace. (A) Direct comparison of ex vivo [^{18}F]ROStrace autoradiography with

DHE fluorescence in the same brain section. Distribution is also comparable with ROStrace fluorescence performed in separate animals. ARG: autoradiography, DHE: dihydroethidium, CX: cortex, HP: hippocampus, CB: cerebellum. (B) LPS treated mice showed significantly higher [^{18}F]ROStrace uptake (* $P < 0.0001$) compared with non-treated animals by ex vivo autoradiography.

Figure 1

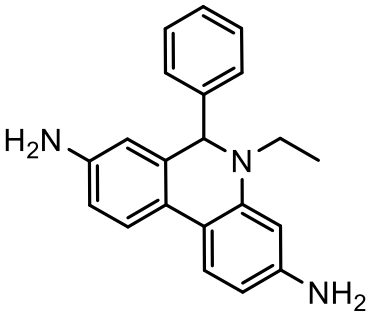

Dihydroethidium (DHE)

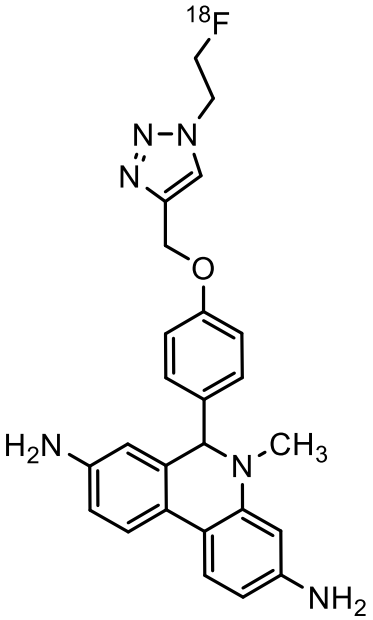

[^{18}F]FDMT

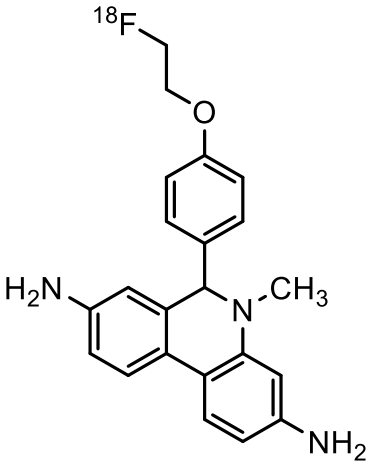

[^{18}F]ROStrace

Scheme 1

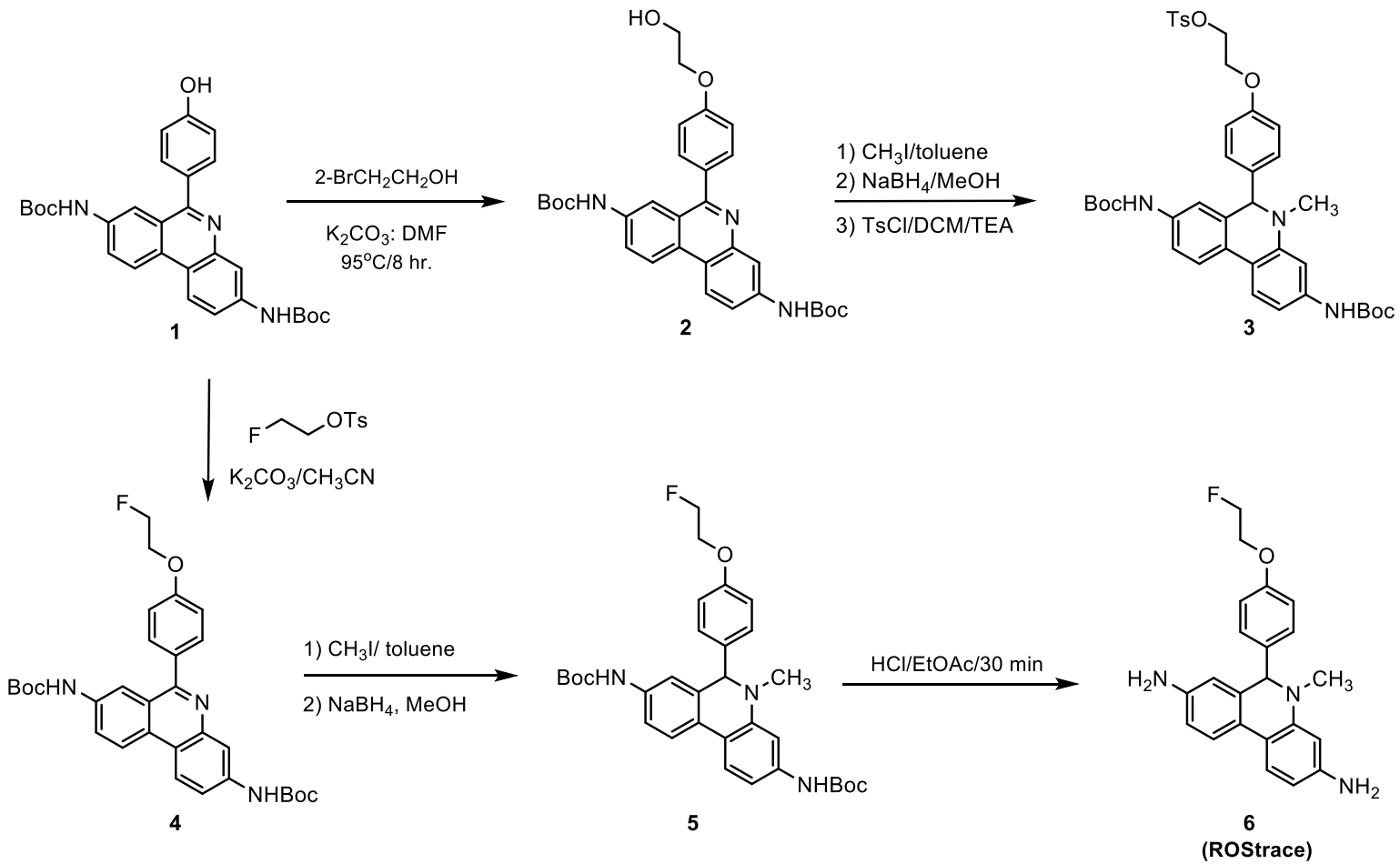
OH
BocHN
N
NHBoc
1
2-BrCH2CH2OH
K2CO3: DMF
95°C/8 hr.
HO
O
2
1) CH3I/toluene
2) NaBH4/MeOH
3) TsCl/DCM/TEA
TsO
CH3
3
F
OTs
K2CO3/CH3CN
4
1) CH3I/ toluene
2) NaBH4, MeOH
5
HCl/EtOAc/30 min
H2N
NH2
6
(ROStrace)

Figure 2

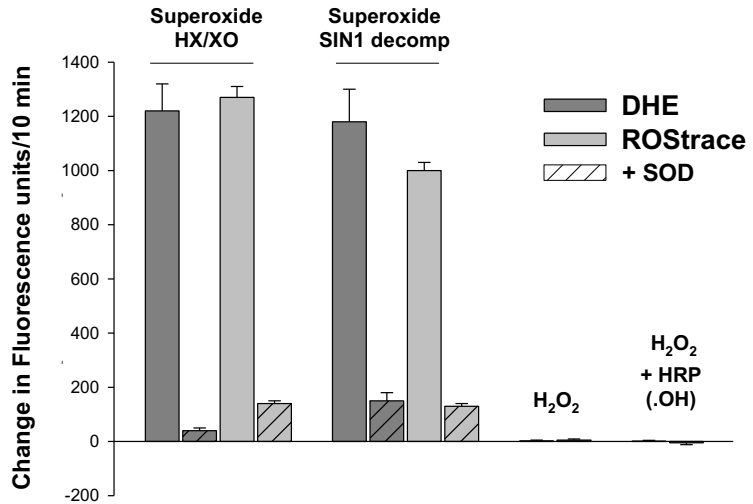
Superoxide
HX/XO
Superoxide
SIN1 decomp
Change in Fluorescence units/10 min
1400
1200
1000
800
600
400
200
0
-200
DHE
ROStrace
+ SOD
H2O2
H2O2
+ HRP
(.OH)

Scheme 2

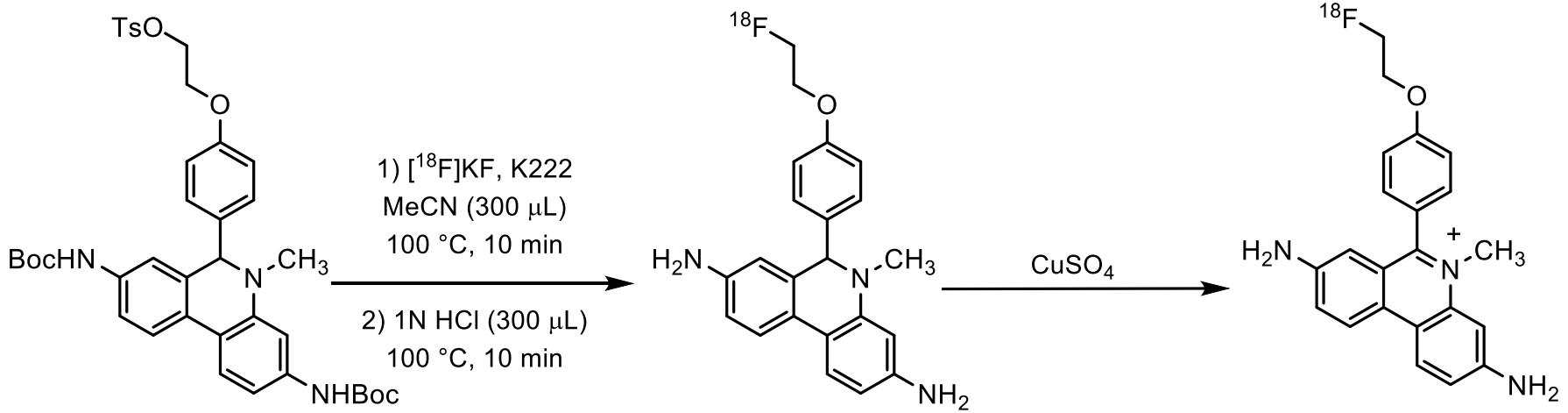

[^{18}F]ROStrace **[^{18}F]ox-ROStrace**

Figure 3

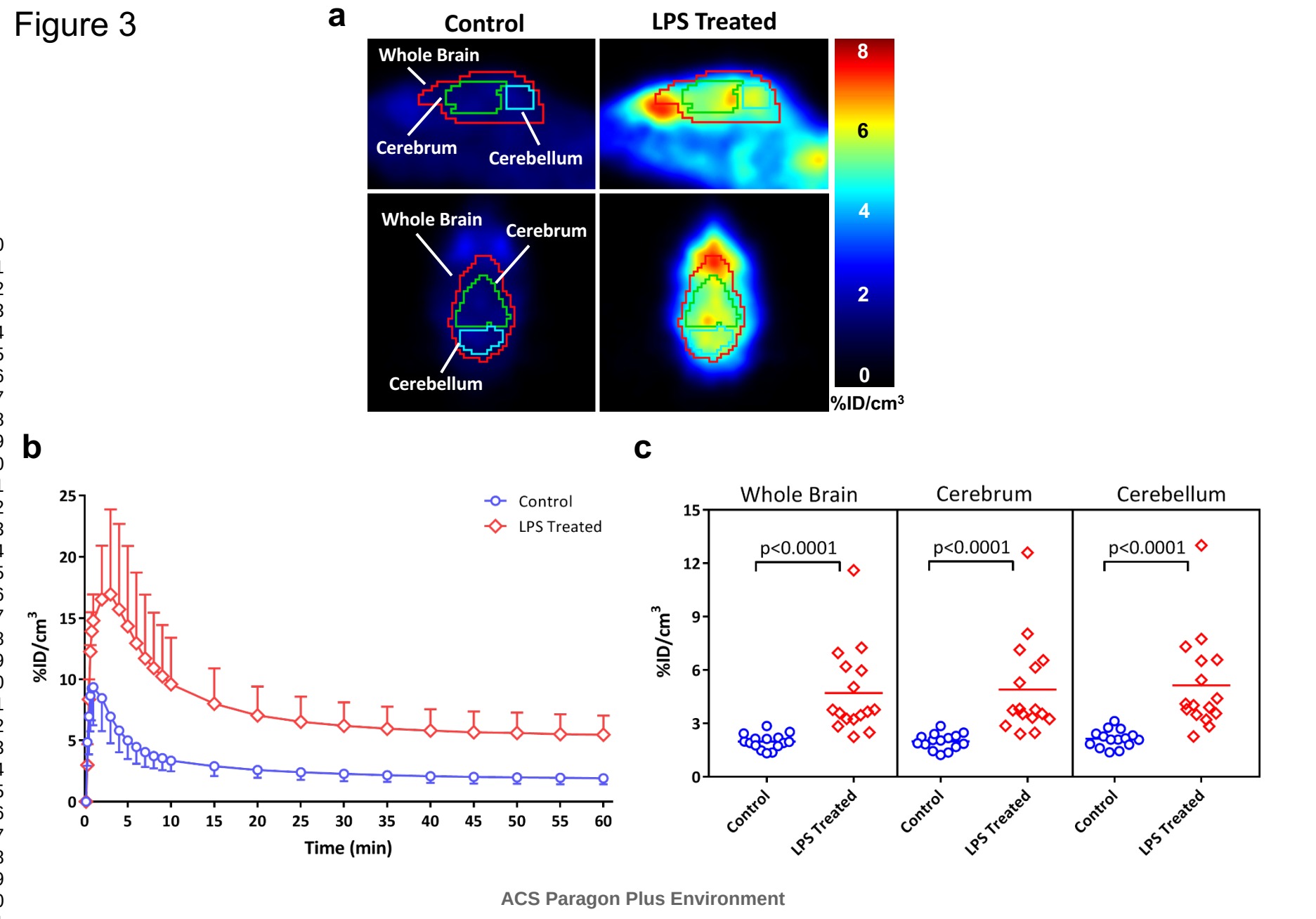
a
Control
LPS Treated
Whole Brain
Cerebrum
Cerebellum
Whole Brain
Cerebrum
Cerebellum
8
6
4
2
0
%ID/cm3
b
Control
LPS Treated
%ID/cm3
Time (min)
c
Whole Brain
Cerebrum
Cerebellum
p<0.0001
p<0.0001
p<0.0001
%ID/cm3
Control
LPS Treated
Control
LPS Treated
Control
LPS Treated

Figure 4

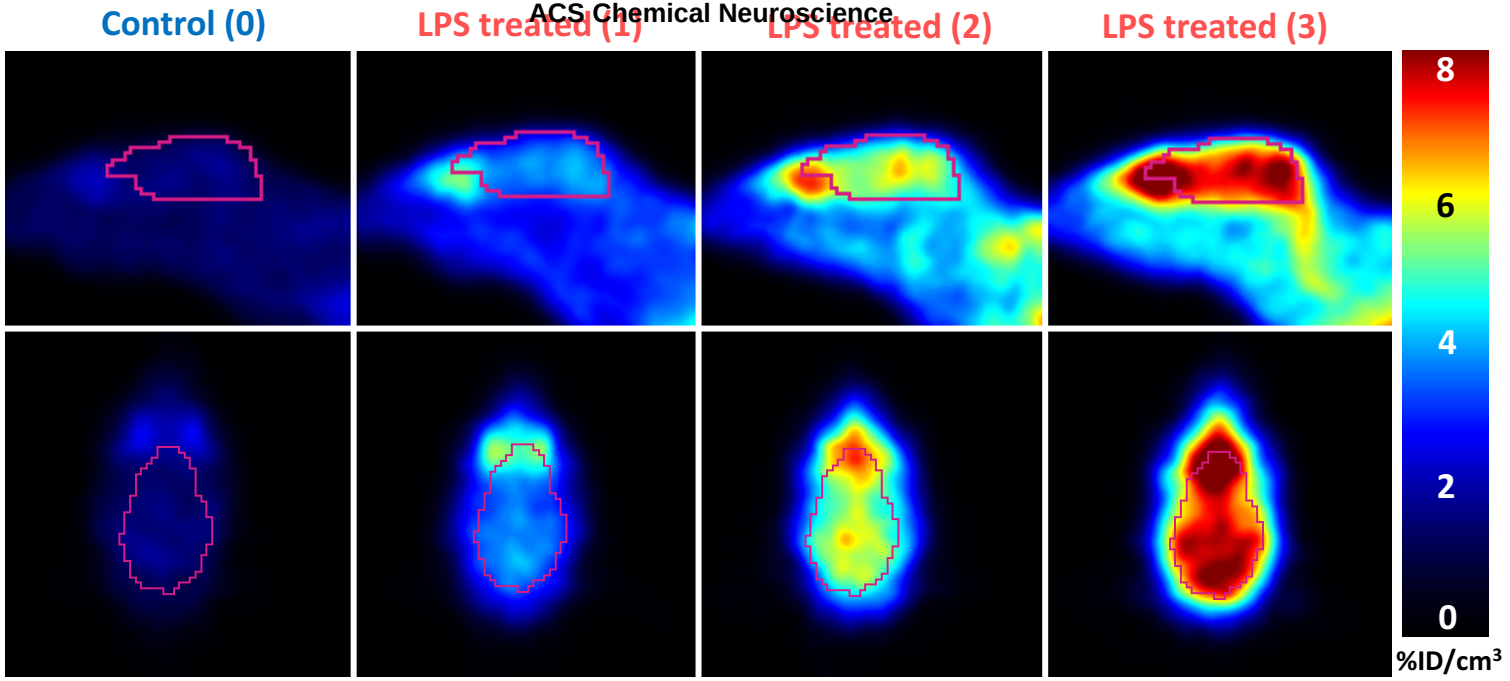
Control (0)
LPS treated (1)
LPS treated (2)
LPS treated (3)
8
6
4
2
0
%ID/cm³

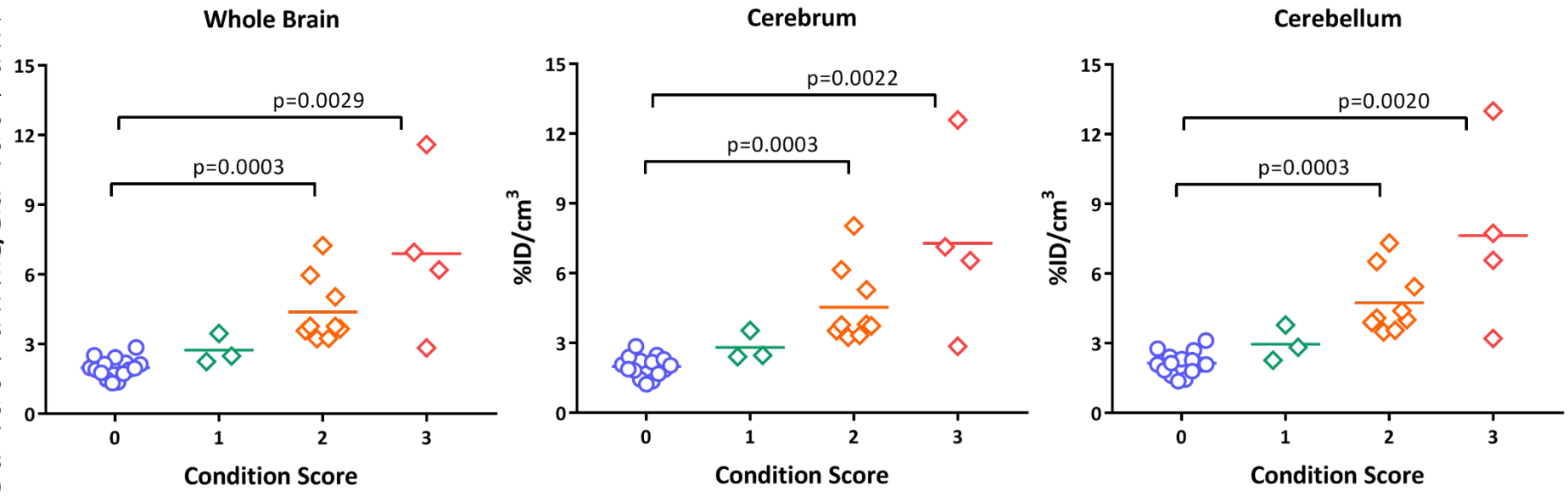
Whole Brain
Cerebrum
Cerebellum
%ID/cm³
p=0.0029
p=0.0003
p=0.0022
p=0.0003
p=0.0020
p=0.0003
15
12
9
6
3
0
0
1
2
3
Condition Score

Figure 5

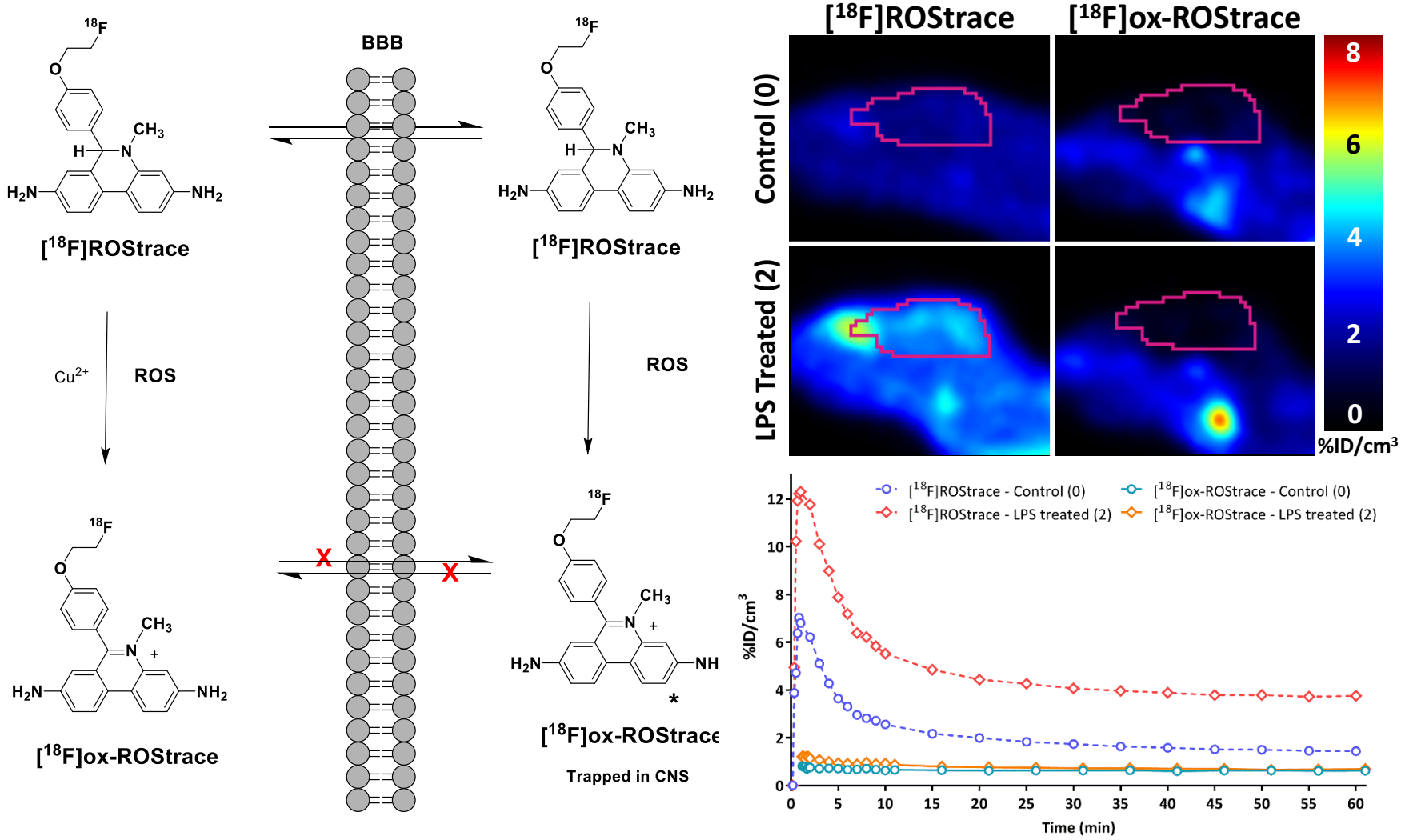
a
BBB
[18F]ROStrace
Cu2+
ROS
[18F]ox-ROStrace
[18F]ROStrace
ROS
[18F]ox-ROStrace
Trapped in CNS
b
[18F]ROStrace
[18F]ox-ROStrace
Control (0)
LPS Treated (2)
8
6
4
2
0
%ID/cm3
[18F]ROStrace - Control (0)
[18F]ROStrace - LPS treated (2)
[18F]ox-ROStrace - Control (0)
[18F]ox-ROStrace - LPS treated (2)
%ID/cm3
Time (min)

Figure 6

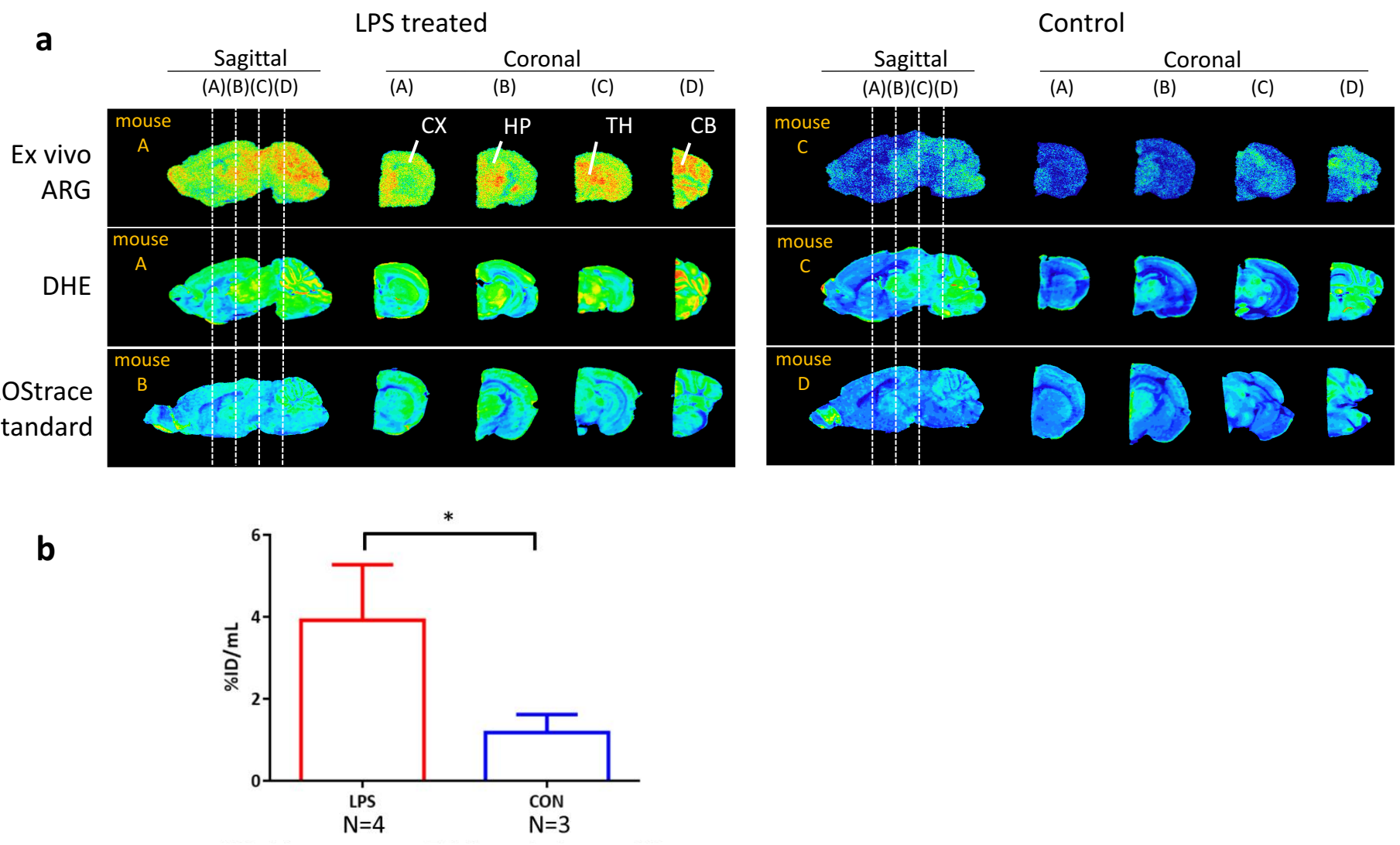
a
LPS treated
Control
Sagittal
(A)(B)(C)(D)
Coronal
(A)
(B)
(C)
(D)
CX
HP
TH
CB
Ex vivo ARG
DHE
ROStrace standard
mouse A
mouse B
mouse C
mouse D
b
%ID/mL
0
2
4
6
*
LPS
N=4
CON
N=3

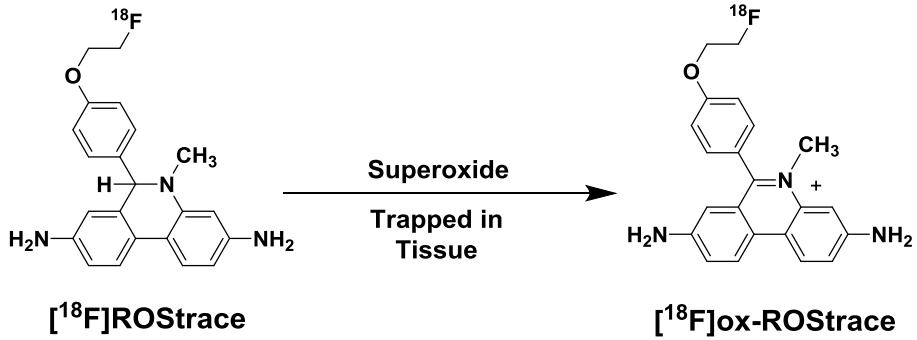

[^{18}F]ROStrace [^{18}F]ox-ROStrace

For Table of Contents Use Only

Development of a PET Radiotracer for Imaging Elevated Levels of Superoxide in Neuroinflammation

Catherine Hou, Chia-Ju Hsieh, Shihong Li, Hsiaoju Lee, Thomas J. Graham, Kuiying Xu, Chi-Chang Weng, Robert K. Doot, Wenhua Chu, Subhasish K. Chakraborty, Laura L. Dugan, Mark A. Mintun, Robert H. Mach